

## THE VLTI ENVIRONMENT AND GENIE

Rainer Wilhelm, Philippe Gitton

European Southern Observatory (ESO), 85748 Garching b. München, Germany

rwillhelm@eso.org, <http://www.eso.org/proj/vlti>

### ABSTRACT

The paper summarizes the expected VLTI performance in the areas most critical to operation of a nulling beam combiner at mid-infrared wavelengths such as GENIE. The data presented were obtained either by measurement or by simulation. When possible, the impact on the GENIE performance in terms of the achievable null depth is computed.

Key words: nulling interferometry; infrared background; fringe tracking; adaptive optics.

### 1. INTRODUCTION

The *Ground-based European Nulling Interferometer Experiment* (GENIE) will serve (1) as a ground-based technology precursor to the spaceborne interferometer Darwin and (2) as a scientific instrument on the *Very Large Telescope Interferometer* (VLTI). The project is a collaboration between the European Space Agency (ESA) and the European Southern Observatory (ESO). Due to its observation principle of nulling interferometry GENIE imposes extremely challenging requirements on the accuracy of thermal background subtraction as well as on the temporal stability of the optical path difference and of the wavefront quality. Hereafter, we address these aspects by summarizing the as-planned VLTI performance in the respective fields. The performances are translated whenever possible into contributions to the null depth in the two GENIE candidate spectral bands L' ( $\lambda_c = 3.74 \mu\text{m}$ ) and N ( $\lambda_c = 10.4 \mu\text{m}$ ). The null depth required by GENIE for both bands is  $10^{-3}$  over a spectral bandwidth  $\Delta\lambda \geq 0.1 \cdot \lambda_c$ . For a general description of the GENIE project the reader is referred to Gondoin et al. (2003).

The data used to estimate the performance were selected such that the seeing experienced (in case of measurements) or assumed (in case of simulations) is close to the median seeing angle  $\alpha = 0.89$  arcsec on Cerro Paranal for the period from 1997 until today (see Figure 1). All seeing values mentioned in

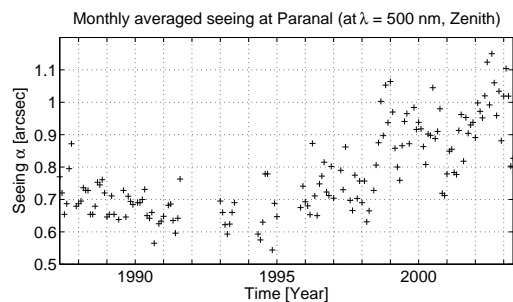


Figure 1. Monthly averaged seeing (in units of arcsec on sky) on Cerro Paranal (for  $\lambda = 500 \text{ nm}$  and Zenith pointing).

this paper are given at a wavelength  $\lambda = 500 \text{ nm}$ .

### 2. THE VLTI ARCHITECTURE IN 2006

By 2006, the VLTI will offer the following facilities (Schöller & Glindemann, 2003):

- Four Unit Telescopes (UTs) (8 m) equipped with adaptive optics (MACAO)
- Two Auxiliary Telescopes (ATs) (1.8 m) equipped with single-feed relay optics and tip/tilt correction (STRAP); relocatable on 30 stations
- Two Auxiliary Telescopes (ATs) (1.8 m) equipped with dual-feed (PRIMA) relay optics and tip/tilt correction (STRAP); relocatable on 30 stations
- Six Delay Lines (DLs) equipped with Variable Curvature Mirrors for pupil re-imaging
- The dual-feed facility PRIMA with two fringe sensor units, laser metrology and star separators on two ATs, i.e. PRIMA “Phase 1”
- Closed-loop optical path difference (OPD) control (“fringe tracking”) with FINITO or PRIMA FSU A/B as fringe sensor units

Table 1. Measured background flux (in units of  $\text{Jy arcsec}^{-2}$ ) on Paranal and La Silla. The background flux comprises the flux of the sky and the (warm) telescope optics (three mirrors in the case of ISAAC; two mirrors in the case of TIMMI2).

| Filter $\Rightarrow$ | Ks     | L    | M-NB | N1                |
|----------------------|--------|------|------|-------------------|
| ISAAC                | 0.0043 | 7.2  | 59.1 | —                 |
| TIMMI2               | —      | 10.0 | —    | 2950 <sup>1</sup> |

### 3. INFRARED THERMAL BACKGROUND

The thermal background level and especially its temporal fluctuations are an important issue for the operation of GENIE. The fluctuations lead to an additional noise contribution other than the photon noise. (Mechanical) chopping or internal modulation techniques can be used to partially subtract the background fluctuations. The knowledge of the temporal behaviour of the background radiation from sky and warm telescope optics is of great importance for proper design of any background subtraction system. Recently, measurements were performed both on Paranal (MIDI on UT) and on La Silla (TIMMI2 on 3.6 m telescope). While the TIMMI2 results are shortly presented below the MIDI results are still being analyzed and will become available soon.

For the TIMMI2 measurements two spectral filters were used: L ( $\lambda_c = 3.6 \mu\text{m}$ ,  $\Delta\lambda = 0.38 \mu\text{m}$ ) and N1 ( $\lambda_c = 7.8 \mu\text{m}$ ,  $\Delta\lambda = 1.2 \mu\text{m}$ ). For absolute photometric calibration the bright star Sirius was observed. For each measurement 350 exposures with a detector integration time of  $T_i = 25$  msec were taken. Table 1 lists the mean background flux level in units of  $\text{Jy arcsec}^{-2}$  (compared with some older data obtained with ISAAC on UT, see Cuby et al. (2000)). The Power Spectral Densities (PSDs) for the two spectral bands are shown in Figure 2. Due to the small number of time samples, the PSD estimation is of poor quality. Nevertheless the PSDs have the shape which one would expect from previous measurements (Käufel et al., 1991; Miyata et al., 1999, 2000): The background noise power is almost constant above a frequency of a few Hz ( $\approx 2$  Hz for L-band,  $\approx 5$  Hz for N1-band) and becomes larger below this frequency. Any background subtraction system should operate at a frequency in the “constant PSD domain”. The distinct peak at a frequency of about 1 Hz present in both PSDs results from periodic temperature variations produced by the closed-cycle cooling system used to cool the detector. It is emphasized that these results can not be directly translated to the case of VLTI/GENIE, mainly because of two reasons: (1) the (warm) VLTI optical train consists of significantly more mirrors (about 25), i.e. has a much higher emissivity, and (2) GENIE will probably differ from TIMMI2 with respect to detector, cooling mechanism etc.

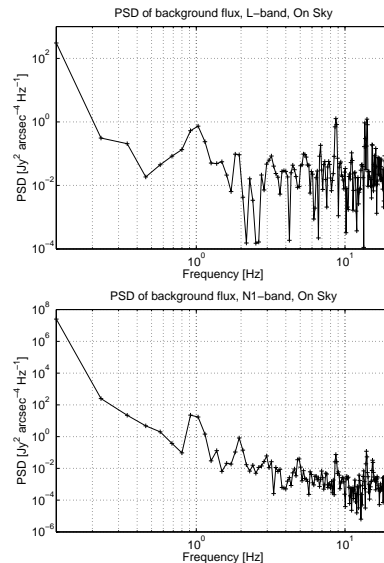


Figure 2. PSD of the background flux (in units of  $\text{Jy}^2 \text{arcsec}^{-4} \text{Hz}^{-1}$ ) measured in La Silla for the L-band (top) and the N1-band (bottom). The corresponding time series consist of only 350 values sampled at a frequency  $f_s = 40$  Hz (length of measurement  $T = 8.75$  sec).

### 4. OPTICAL PATH DIFFERENCE CONTROL

Fast compensation of the optical path difference (OPD) variations is very important for a successful operation of GENIE. Figure 3 shows the block diagram of the VLTI OPD control (fringe tracking) loop. The components of the loop are the Fringe Sensor Unit (FSU), the OPD Controller (OPDC) and the VLTI Delay Line (DL). The FSU measures the phase and group delay between two or more beams. The measured signal is sent to the OPDC which then computes and applies a correction signal to the DL in order to minimize the residual OPD. In 2006, there will be two types of FSUs available: (a) FINITO (Fringe Tracking Instrument of Nice and Torino) operating in the H-band and (b) PRIMA FSU (dual implementation) operating in K-band. FINITO can measure the OPDs between three beams. While handling only two beams the PRIMA FSUs will provide a better sensitivity (by two magnitudes) than FINITO. The latter is not really an advantage in the specific case of GENIE since the central star will be very bright anyway.

To estimate the expected OPD control performance a simulation using the *VLTI Integrated Model* (Müller & Wilhelm, 2002) was performed. Figure 4 shows the PSDs of the individual OPD noise contributions from atmospheric turbulence, FSU and DL, each before and after closed-loop correction.

<sup>1</sup>Photometric calibration doubtful because of modified detector integration times during measurement.

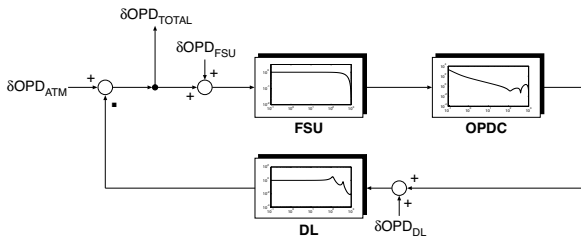


Figure 3. Block diagram of the VLTI fringe tracking loop.  $\delta OPD_{ATM}$ ,  $\delta OPD_{FSU}$  and  $\delta OPD_{DL}$  denote the atmospheric OPD (“piston”), the FSU measurement noise (at FSU input) and the DL noise (at DL input).  $\delta OPD_{TOTAL}$  is the total residual OPD.

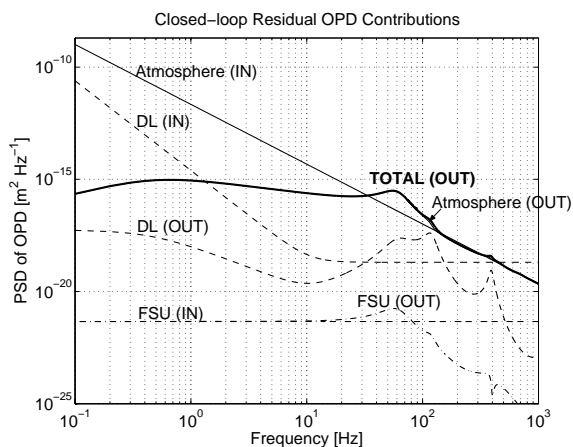


Figure 4. PSDs of residual OPD contributions (after closed-loop control) for the three OPD noise sources in the fringe tracking loop. Simulation parameters as listed in Table 2 with  $f_S = 2$  kHz.

Table 2 lists the standard deviations of the residual OPD for different loop sampling frequencies  $f_S = 2$  kHz, 4 kHz and 8 kHz. Currently the DL electronics imposes an upper limit of  $f_S = 2$  kHz. Knowing the standard deviation  $\sigma_{TOTAL}$  of the residual OPD one can estimate the contribution to the null depth by the relation (Mennesson et al., 2002)

$$\bar{N} = \frac{1}{4} \cdot \left( \frac{2\pi}{\lambda} \right)^2 \cdot \sigma_{TOTAL}^2 \quad (1)$$

The resulting null depths in the two GENIE candidate bands L’ and N are given in Table 2. The simulation results show that increasing the loop sampling frequency above its nominal value of 2 kHz does not significantly improve the residual OPD error (and the resulting null depth). The closed-loop performance is limited by the DL transfer function which rapidly drops off after its first resonance frequency at about 120 Hz. Being clearly dominated by the atmospheric contribution, the obtained residual OPD values are above the accuracy required by GENIE to reach a null depth of  $\bar{N}_{max} = 10^{-3}$ .

Table 2. Simulated standard deviations of the contributions to the residual OPD for an exposure time  $T = 2$  sec and different loop sampling frequencies  $f_S$ . The simulation assumed usage of a PRIMA FSU as fringe sensor. The table also gives the contributions to the null depth in the two GENIE candidate spectral bands L’ and N. The values in **bold type-face** correspond to the maximum sampling frequency  $f_S = 2$  kHz achievable with the current DL electronics. Simulation parameters: UT baseline  $B \approx 100$  m, magnitude  $m_K = 2$ , Strehl ratio  $\bar{S}_K = 0.36$  (i.e. expected MACAO performance for a seeing  $\alpha = 1$  arcsec, see Section 5), FSU integration time  $T_i = 500 \mu\text{sec}$ , FSU readout noise  $RON = 20 e^-$ , FSU fringe visibility  $V = 75\%$ , Fried parameter  $r_0 = 60$  cm in K-band (corresponds to a seeing of  $\alpha = 1$  arcsec), mean wind speed  $\bar{v} = 11.6 \text{ m sec}^{-1}$ .

| $f_S$            | 2 kHz                                  | 4 kHz                | 8 kHz                |
|------------------|--|----------------------|----------------------|
| $\sigma_{FSU}$   | <b>0.3 nm</b>                          | 0.3 nm               | 0.3 nm               |
| $\sigma_{DL}$    | <b>15.5 nm</b>                         | 17.0 nm              | 18.3 nm              |
| $\sigma_{ATM}$   | <b>157.3 nm</b>                        | 146.3 nm             | 136.2 nm             |
| $\sigma_{TOTAL}$ | <b>158.0 nm</b>                        | 147.3 nm             | 137.5 nm             |
| $\bar{N}_{L'}$   | <b><math>1.76 \cdot 10^{-2}</math></b> | $1.53 \cdot 10^{-2}$ | $1.33 \cdot 10^{-2}$ |
| $\bar{N}_N$      | <b><math>2.28 \cdot 10^{-3}</math></b> | $1.98 \cdot 10^{-3}$ | $1.73 \cdot 10^{-3}$ |

## 5. WAVEFRONT CORRECTION SYSTEMS

GENIE will benefit from the existing VLTI closed-loop wavefront correction systems. The ATs will be equipped with the fast tip/tilt correction system STRAP (System for Tip/Tilt Removal with Avalanche Photodiodes, currently installed on UTs) whereas the adaptive optics system MACAO (Multiple Applications Curvature Adaptive Optics) will perform correction of both tip/tilt and higher-order modes on the UTs. In the case of GENIE both systems will serve the purpose to optimize and, even more important, equalize the flux of different beams coupled into the single-mode fiber of the nulling beam combiner.

Both systems sense the wavefront at visible wavelengths. Physically, the measurement of the wavefront aberrations is performed at the level of the UT’s or AT’s coude focus — a long focal length focus at underground level which remains fixed in space during azimuthal rotation of the telescopes. In the case of STRAP the tip/tilt correction signal is applied to a mirror located in a pupil plane (M2 for UT, M6 for AT). MACAO’s corrective optics consists of a deformable mirror with 60 actuators mounted on a tip/tilt stage situated in a UT pupil plane at the location of the so-called M8 mirror.

Since the wavefront sensing performed by STRAP and MACAO is *not* done at the location of the instrument, i.e. in the interferometric laboratory, but at telescope level, an additional tip/tilt error due to

air turbulence in the underground light path will add to the residual tip/tilt of both correction systems. It is planned to reduce this additional low frequency tip-tilt error by implementing a specific closed loop control system (IRIS – *InfraRed Image Sensor*). It would be formed by an infrared sensor located in the interferometric laboratory that simultaneously monitors up to four beams (i.e. four telescopes). The error signal will be fed at a typical rate of  $f_S = 0.5$  Hz to existing actuators located in the coudé area of the corresponding telescopes.

Hereafter we describe the expected performances of STRAP, MACAO and IRIS and their impact on the null depth. For STRAP and MACAO we consider the “GENIE-case” of a *bright guide star*. Note that both STRAP and MACAO use neutral density filters for stars brighter than magnitude  $m_V = 9$ .

### 5.1. Tip/tilt correction

Figure 5 shows the PSDs of the residual tip/tilt errors obtained using STRAP on UTs. The data was collected during a commissioning run in early 2002. Important parameters were the seeing  $\alpha = 0.85$  arcsec, the guide star magnitude  $m_V = 11.2$ , and the M2 update frequency  $f_{M2} = 100$  Hz. The standard deviations of the residual tip/tilt (on sky) for an exposure time of  $T = 2$  sec are  $\sigma_{TIP} = 17.9$  marcsec and  $\sigma_{TILT} = 18.6$  marcsec (see Table 3). The peak in the PSD at a frequency of 18 Hz was identified as a mechanical resonance of the actuated mirror M2.

With the installation of MACAO on the UTs, STRAP will be moved to the ATs. Data for this case is not yet available. Important differences between the STRAP on UT/AT cases are the size of the actuated mirror (UT:  $\varnothing_{M2} = 1.1$  m, AT:  $\varnothing_{M6} = 13.8$  cm), the effective focal length at the coudé focus which determines the scale factor between a tip/tilt angle on the sky and the resulting lateral displacement on the STRAP sensor (UT:  $f \approx 415$  m, AT:  $f \approx 62$  m), and the size of the entrance aperture (UT:  $\varnothing_{M1} = 8$  m, AT:  $\varnothing_{M1} = 1.8$  m). Due to the smaller aperture of the ATs the tip/tilt caused by atmospheric turbulence (prior to correction by STRAP) will be larger than for the UTs. This is because wavefront distortions tend to have larger slope changes over small scales.

Figure 6 shows the PSDs of the residual tip/tilt errors obtained using MACAO on UTs. The results were obtained by a simulation performed by the *ESO Adaptive Optics Group*. Important simulation parameters were the seeing  $\alpha = 1$  arcsec, the guide star magnitude  $m_V = 9$ , the MACAO sampling frequency (or “command frequency”)  $f_{MACAO} = 350$  Hz, the simulation sampling frequency  $f_S = 2.1$  kHz, the simulation total time  $T = 2$  sec. The peaks in the PSDs at frequencies of 350 Hz, 700 Hz and 1050 Hz (all multiples of the command frequency  $f_{MACAO}$ ) are resonances resulting from the fact that the MACAO commands are applied as step-

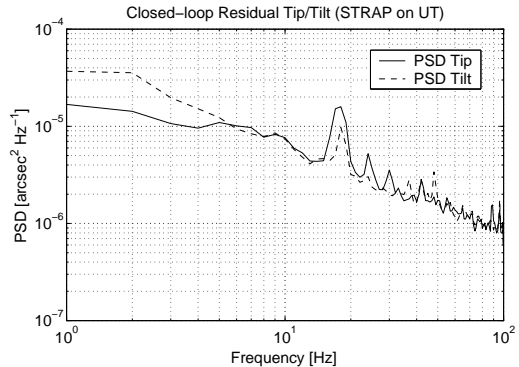


Figure 5. PSD of the measured residual tip/tilt (on sky) after closed-loop correction by STRAP on UT3. The seeing and guide star magnitude are  $\alpha = 0.85$  arcsec and  $m_V = 11.2$ , respectively.

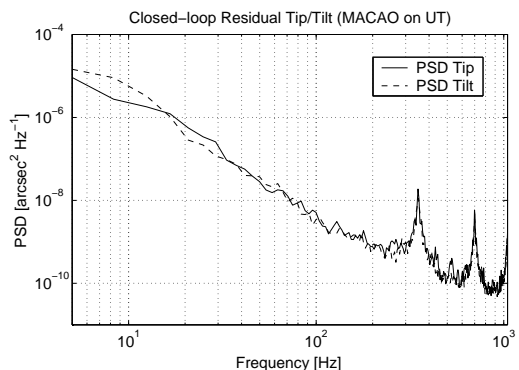


Figure 6. PSD of the simulated residual tip/tilt (on sky) after closed-loop correction by MACAO on a UT. The simulation considered a bright star case ( $m_V = 9$ ) and a seeing  $\alpha = 1$  arcsec.

functions. The standard deviations of the residual tip/tilt (on sky) for an exposure time of  $T = 2$  sec are  $\sigma_{TIP} = 12.7$  marcsec and  $\sigma_{TILT} = 13.1$  marcsec (see Table 3).

Figure 7 displays the PSDs of the additional tip/tilt contribution of the underground light path (with and without correction by IRIS). The data was collected under representative conditions in Paranal. The PSDs of the *residual* tip/tilt were computed assuming a simplified model of IRIS (perfect correction with a closed-loop bandwidth of 0.1 Hz). The standard deviations of the residual tip/tilt (on sky) for an exposure time of  $T = 2$  sec are  $\sigma_{TIP} = 8.7$  marcsec and  $\sigma_{TILT} = 9.8$  marcsec (see Table 3).

Assuming a nulling beam combiner which uses single-mode fibers as modal filters the null depth due to a residual tilt  $\sigma_\theta$  (on sky) can be estimated by (Ménnesson et al., 2002)

$$\bar{N} = \frac{1}{64} \cdot \left( \frac{\pi D \sigma_\theta}{\lambda} \right)^4 \quad (2)$$

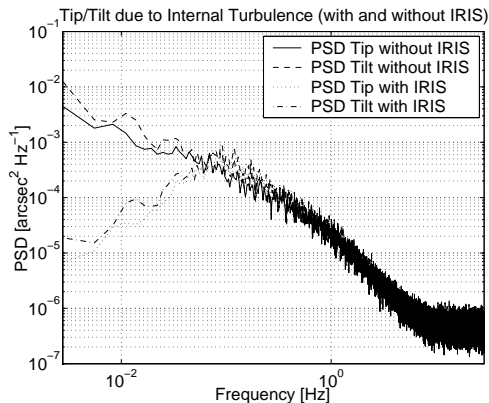


Figure 7. PSD of the residual tip/tilt (in units of arcsec on sky) due to internal turbulence along the underground light path (measured) and after closed-loop correction by IRIS (computed assuming a perfect correction with a closed-loop bandwidth of 0.1 Hz).

Table 3. Standard deviations of measured or simulated residual tip/tilt errors (on sky) of the three wavefront correction systems STRAP, MACAO and IRIS (all on UT), and the resulting contributions to the null depth in the two candidate spectral bands L' and N. The IRIS contribution has to be added to either the STRAP or MACAO residual tip/tilt. The total time for which the standard deviations are computed is  $T = 2$  sec. The seeing angles are  $\alpha = 0.85$  arcsec for STRAP and  $\alpha = 1$  arcsec for MACAO.

|                 | STRAP<br>on UT      | MACAO<br>on UT      | IRIS<br>on UT       |
|-----------------|---------------------|---------------------|---------------------|
| $\sigma_{TIP}$  | 17.9 marcsec        | 12.7 marcsec        | 8.7 marcsec         |
| $\sigma_{TILT}$ | 18.6 marcsec        | 13.1 marcsec        | 9.8 marcsec         |
| $\bar{N}_{L'}$  | $2.0 \cdot 10^{-3}$ | $4.9 \cdot 10^{-4}$ | $1.3 \cdot 10^{-4}$ |
| $\bar{N}_N$     | $3.3 \cdot 10^{-5}$ | $8.2 \cdot 10^{-6}$ | $2.3 \cdot 10^{-6}$ |

with the diameter  $D$  of the entrance pupil. Table 3 lists the contributions to the null depth in the two GENIE candidate bands computed using Equation 2. The value of interest in the UT case is the combined contribution of MACAO and IRIS. It stays well below  $10^{-5}$  in the N-band. In contrast, the corresponding value in the L'-band is already about 50% of the maximum allowed null depth  $\bar{N}_{max} = 10^{-3}$ .

## 5.2. Higher-order modes correction

As mentioned earlier, only the beams delivered by the UTs will benefit from a higher-order modes correction. Figure 8 shows the PSD of the Strehl ratio  $S_K$  in K-band obtained using MACAO on UTs. The data result from the MACAO simulation mentioned in Section 5.1. The mean value of the Strehl ratio in K-band is  $\bar{S}_K = 0.36$  which translates into the values

$\bar{S}_{L'} = 0.70$  and  $\bar{S}_N = 0.95$  in the two GENIE candidate bands. These values exclude the tip/tilt contribution. In a nulling interferometer which employs single-mode fibers as modal filters the null depth mainly depends on the *temporal stability* and not so much on the mean value of the Strehl ratio. If one assumes the coupling efficiency into a single-mode fiber to be equal to the Strehl ratio of the beam, the contribution to the null depth is given by (Meneson et al., 2002)

$$\bar{N} = \frac{1}{16} \cdot \frac{2\sigma_S^2}{\bar{S}^2} \quad (3)$$

where  $\bar{S}$  is the mean Strehl ratio and  $\sigma_S^2$  is the variance of the Strehl ratio of an individual beam. Assuming uncorrelated Strehl ratio fluctuations in both beams the term  $2\sigma_S^2$  in the numerator of Equation 3 corresponds to the variance of the difference in Strehl ratio between the two beams. The MACAO simulation yields a standard deviation of the Strehl ratio in K-band for an exposure time  $T = 2$  sec of  $\sigma_{S,K} = 6.3 \cdot 10^{-2}$ . The corresponding values in the L' and N band are given in Table 4.

The contributions to the null depth in the L' and N-band resulting from Strehl ratio fluctuations are listed in Table 4. The result is similar to that in the case of residual tip/tilt. While the N-band contribution  $\bar{N}_N$  is more than two orders of magnitude lower than the maximum allowed value  $\bar{N}_{max} = 10^{-3}$ , the L'-band value  $\bar{N}_{L'}$  reaches 50% of  $\bar{N}_{max}$ .

In the case of the ATs which lack a higher-order correction system there will also be a contribution to the null depth caused by Strehl ratio fluctuations. While the uncorrected mean Strehl ratio can easily be calculated ( $\bar{S}_K = 0.44$ ; excluding tip/tilt) we currently have no estimate of the variance  $\sigma_S^2$  of the Strehl ratio fluctuations.

A successful commissioning run of a first MACAO unit on UT2 took place in April 2003<sup>2</sup>. Without optimization a mean long-exposure Strehl ratio  $\bar{S}_K \approx 0.55$  was achieved for a seeing  $\alpha = 0.8$  arcsec and a guide star magnitude  $m_V = 9.9$ . The system operated at a closed-loop bandwidth (or *correction bandwidth*) of 30 Hz. Data on the variations of the Strehl ratio with time are not yet available.

## 6. CONCLUSION

We have addressed three aspects of the “VLTI environment” which are critical for the operation of GENIE: the level and temporal stability of the infrared background, optical path difference control and wavefront correction. It is emphasized that the conclusions drawn below have a preliminary character. Most of the performance estimates presented

<sup>2</sup><http://www.eso.org/outreach/press-rel/pr-2003/pr-11-03.html>

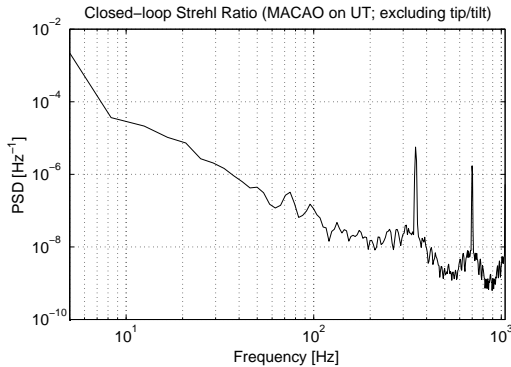


Figure 8. PSD of the simulated Strehl ratio  $S_K$  (excluding tip/tilt) after closed-loop correction by MACAO on a UT. The simulation considered a bright star case ( $m_V = 9$ ) and a seeing  $\alpha = 1$  arcsec.

Table 4. Mean value and standard deviation (over  $T = 2$  sec) of the Strehl ratio (after correction by MACAO on UT) and its contribution to the null depth in the two GENIE candidate spectral bands  $L'$  and  $N$ . The seeing angle is  $\alpha = 1$  arcsec.

|      | $\bar{S}$ | $\sigma_S$          | $\bar{N}$           |
|------|-----------|---------------------|---------------------|
| $L'$ | 0.70      | $4.4 \cdot 10^{-2}$ | $4.9 \cdot 10^{-4}$ |
| $N$  | 0.95      | $7.9 \cdot 10^{-3}$ | $8.5 \cdot 10^{-6}$ |

were obtained by simulation and not by measurements.

Regarding the *infrared background* a conclusion can not be drawn yet. Data collected with MIDI on Paranal in the N-band are still being processed. The TIMMI2 data from La Silla in the L- and N1-band are not of sufficient quality to fully qualify the background environment. More and refined measurements are needed. In terms of *OPD control*, the expected residual OPD values are far above the accuracy required in both GENIE candidate spectral bands  $L'$  and  $N$ . Therefore GENIE will need its own fast OPD control system as a second-stage correction system in addition to the standard VLTI fringe tracking loop. Concerning the performance of the VLTI *wavefront correction* systems on UTs a different conclusion applies for the two bands: While the performance in the N-band is sufficiently high, a GENIE operating in the  $L'$ -band will require an additional closed-loop amplitude matching control system to achieve a null depth of  $10^{-3}$ .

Future work will concentrate on refining the specifications of the VLTI-GENIE interface. Important steps are the gradual replacement of simulated data by measured as-built data as well as the extension of the performance estimates towards the ATs.

## ACKNOWLEDGMENTS

The authors wish to thank Ralf Siebenmorgen and Hans-Ulrich Käuffl for their support on measurement and data analysis of the infrared background data. The contribution of MACAO simulation results by Enrico Fedrigo is gratefully acknowledged. Thanks also to Serge Menardi and Martin Dimmler for numerous discussions on the topic of OPD control.

## REFERENCES

- Cuby J. G., Lidman C., Moutou C., 2000, ISAAC: 18 Months of Paranal Science Operations, *ESO Messenger*, Vol. 101, pp. 2-8
- Gondoin P. et al., 2003, The GENIE Project, in: *these proceedings*
- Käuffl H. U., Bouchet P., Van Dijsseldonk A., Weilenmann U., 1991, A Sky-noise Measurement and its Implication for Ground-based Infrared Astronomy in the 10  $\mu$ m Atmospheric Window, *Experimental Astronomy 2*, pp. 115-122
- Mennesson B., Ollivier M., Ruilier C., 2002, Use of single-mode waveguides to correct the optical defects of a nulling interferometer, *J. Opt. Soc. Am. A*, Vol. 19, No. 3, pp. 596-602, 2002
- Miyata T. et al., 1999, MICS: A New Mid-Infrared Camera and Spectrometer for Ground-based Astronomy, *Publ. Astr. Soc. Pac.*, Vol. 111, pp. 750-764
- Miyata T. et al., 2000, Midinfrared Camera and Spectrometer (MICS) and Sky Noise Measurements in the N-band, in: *Optical and IR Telescope Instrumentation and Detectors*, Proc. SPIE 4008, pp. 842-852
- Müller M., Wilhelm R., 2002, Integrated modeling for the VLTI, in: *Interferometry for Optical Astronomy II*, Proc. SPIE 4838, pp. 881-892
- Schöller M., Glindemann A., 2003, in: *these proceedings*